Supplementary Methods

Radiosonde Station Selection

Zonal wind for each day and pressure is estimated from the radiosonde reported wind (a vector) by multiplying the wind speed by negative of the sine of the wind direction. To calculate a station's monthly zonal wind , we required at least 12 launches with good data (both wind speed and direction). To calculate a seasonal value, we required at least two of the three monthly values, and for an annual anomaly we required all four valid seasons. To minimize trend errors, each station needed at least five annual averages in the first and last decade. We required a station to satisfy these criteria at seven mandatory tropospheric/lower stratospheric levels: 850, 700, 500, 300, 200, 150, 100 hPa. Based on this requirement, the average number of missing days per month at 500 hPa for 1970-2005 is two (Supplementary Figure 1). Furthermore, nearly 91% of the total number of months have ≥ 24 valid launches per month. Valid data for other pressure levels and the satellite time period are similar.

We find negligible difference between 0000 and 1200 UTC wind trends. As Supplementary Figure 2 shows, the trend difference between stations that observe at both 0000 and 1200 UTC is typically between +/- 0.05 m [s-decade]$^{-1}$, with a mean ~0 m [s-decade]$^{-1}$. We therefore used trends from either or both observing times, as available, at each station.

Data Interpolation and Trend Estimation

We estimated wind shear trends in two ways. First, we assigned each station's monthly zonal wind anomaly for a given pressure to that station's nearest grid point (with

no interpolation). When more than one station matched the same grid point, that grid point's monthly value was estimated as the average of the available station values (many grid points contain no data). After averaging the monthly values to obtain an annual average, a zonal mean annual trend and its uncertainty were then estimated at each grid point[1]. The alternative procedure was to compute a trend first at each station from annual mean data, then bin these trends onto the grid according to the previous procedure[2]. Because both methodologies yielded similar results, only the former is shown.

Uncertainty Estimation

The sampling uncertainty in wind-estimated temperature trends ($\hat{\bar{T}}_t$) is computed by estimating the mean annual wind-estimated temperature gradient trend for each station and pressure layer, $\Delta\hat{\bar{T}}_t[s,p]$. For each 5° latitude, the variance of $\Delta\hat{\bar{T}}_t[\phi,p]$ is computed as

$$Var(\Delta\hat{\bar{T}}_t[\phi,p]) = \frac{\sigma^2[\phi,p]}{n-1}, \qquad \text{(S1)}$$

where $\sigma^2[\phi,p]$ is the sample variance of $\Delta\hat{\bar{T}}_t[s,p]$ for the n valid grid values at latitude ϕ. At least 10 stations distributed into 2 latitude grids are required to estimate (S1); otherwise, adjacent latitude grids up to 10° latitude (+/- 1 grid) away are used to help estimate $\sigma^2[\phi,p]$ (though *n* in the denominator of (S1) is still equal to the number of grid points at ϕ itself).

The error estimate, $Var(\Delta\hat{\bar{T}}_t[\phi,p])$, is then integrated over latitude—including the squared uncertainty of the boundary value where integration commences—to obtain

$Var(\Delta\hat{\overline{T}}_t[\phi,p])$. We assume latitudinal independence of $\Delta\hat{\overline{T}}_t[\phi,p]$ such that the 1-σ uncertainty in the wind-estimated $\overline{T}$ trend is obtained by taking the square root of $Var(\Delta\hat{\overline{T}}_t[\phi,p])$ at each latitude. Supplementary Figure 3 shows both wind-estimated temperature trend 2-σ uncertainties. The uncertainty peaks in the SH because it is additive from the boundary latitude (62.5°N). Choosing a different BC will yield a different result.

Our choice of (S1) above to estimate the uncertainty in wind shear and (through thermal wind balance) the implied $\overline{T}$ trends, deserves explanation. Since it is based on the scatter among individual stations (or grid averages of nearby stations), it reflects both spatial variability of the trend and random errors in the estimation of the trend at individual locations due to errors or microscale wind variations. The latter include bias changes at individual stations, if they vary randomly from one station to the next. If a systematic bias toward (say) more easterly shear were prevalent across the entire network, however, our error estimate would not include this; previous studies have not found evidence for such a tendency, but this remains a limitation of our analysis. Our uncertainty estimate also does not include the uncertainty of fit of a straight line to the data associated with natural fluctuations in time of the actual zonal-mean wind itself. We do not want to include this "uncertainty" because it is relevant only for deciding whether the trend was physically noteworthy, rather than the simple question of whether it occurred. The key question behind our study is whether the warming in the troposphere during a specific time period was consistent with that reported at the surface during the same time period and with the same natural (e.g. ENSO) fluctuations.

The boundary uncertainty was estimated by varying boundary assumptions. For example, if the IUK or RAOBCORE boundary is used, the 1970-2005 warming maximum decreases to 0.35 and 0.55 K decade^{-1}, respectively (Supplementary Figure 4). For 1979-2005, the warming maximum decreases by ~0.10 K decade^{-1} (Supplementary Figure 5). As shown in Supplementary Figures 6 and 7, if the boundary latitude is varied from 62.5° N (which corresponds to the latitude of the maximum number of IGRA stations), peak warming ranges from 0.35 to 0.45 (0.45 to 0.75) K decade^{-1} for 1979-2005 (1970-2005). The higher latitude BCs, however, contain substantially fewer IGRA stations—at 67.5°N (72.5) there are ~50% (25%) of the number of stations available at 62.5°N.

The total uncertainty of $\hat{\overline{T}}_{t\max}$ is obtained by adding the three error sources (sampling uncertainty from (1) + BC latitude + BC data set) in quadrature. For 1979-2005 (1970-2005), the total uncertainty is $\sqrt{0.25^2 + 0.1^2 + 0.1^2} = 0.29$ K decade^{-1} ($\sqrt{0.20^2 + 0.3^2 + 0.3^2} = 0.47$).

Neglect of Moisture

Although the thermal wind equation relates layer virtual temperature gradients (which depend on moisture) to wind shear, we neglect moisture because 1. moisture effects on temperature are small; and 2. the observed trend in moisture is small. Supplementary Figure 8 shows the difference between wind-estimated virtual layer temperature trends (as in Fig. 3d) and wind-estimated layer temperature trends. Using the definition of virtual temperature, $T_v = T(1 + 0.61q)$, this difference (i.e. the error in neglecting

moisture) is estimated as the trend in $(0.61\bar{q}\bar{T})$, where $\bar{q}$ is layer specific humidity. We use NCEP/NCAR Reanalysis data to estimate this error, but because Reanalysis specific humidity extends only to 300 hPa, we assume saturation and estimate $\bar{q}$ from the Clausius-Clapeyron equation and $\bar{T}$ for all pressure levels. Supplementary Figure 8 shows that the maximum error in neglecting moisture in the wind-estimated temperature trends is ~0.01 K decade^{-1} close to the surface in the tropics and subtropics. Near the area of wind-estimated maximum tropical tropospheric warming, the error is < 0.001 K decade^{-1}, which is two orders of magnitude smaller than the estimated trend. Hence, moisture is neglected.

Climate Model Selection and Additional Model Results

The six models selected for this study are the UKMO-HadCM3, GISS-EH, GISS-ER, CNRM-CM3, MIROC3.2 medres and MIROC3.2 hires (Supplementary Table 1). These six models were chosen because they include well-mixed greenhouse gases, sulfate aerosol direct effects, and tropospheric and stratospheric ozone (most also include additional forcings, like black carbon and volcanic aerosols, but this was not required)[3]. Furthermore, these six models predict surface warming in the tropics similar in magnitude to that observed (within 0.05 K decade^{-1})[4]. Data through 1999 come from the 20th Century Climate Change experiment. Data from 2000-2005 are from the Special Report on Emission Scenarios (SRES) A1B experiment (i.e. 720 ppm stabilization experiment)[5]. Because some of these models only contain one realization, only the first run for each model is analyzed.

Supplementary Figure 9 shows in greater detail the $\hat{\bar{T}}_t$ reconstructed for one climate

5□

model, using the same data mask as the observations. Clearly, the reconstruction of the model's own temperature trend field is very good even across the equator, and in detail at all latitudes. Most of the deviations are due to the incomplete sampling of the atmosphere. The reason this reconstruction works well even near the equator is that one is estimating temperature gradients from wind; going in the reverse direction would not work close to the equator (since $1/f \rightarrow \infty$).

As mentioned in the main text, although the 1970-2005 $\hat{\bar{T}}_{t\max}$ is stronger than the model average (and significantly warmer than the ensemble mean at the 95% confidence level), it is within the range simulated by some CMIP3 models. For example, CCCma-CGCM3.1(T63) $\hat{\bar{T}}_{t\max}$~0.65 K decade^{-1} for 1970-2005, which agrees with that based on the winds. Furthermore, the difference in $\hat{\bar{T}}_{t\max}$ of ~0.2 K decade^{-1} between the two time periods is almost within the spread among individual model runs, which ranged from -0.35 K decade^{-1} in the GFDL-CM2.1 to +0.15 K decade^{-1} in the UKMO-HadGEM1. This difference is also less than the estimated uncertainty of either trend. Thus the departures of $\hat{\bar{T}}_{t\max}$ from the model averages for the two periods are consistent with either natural variability or recognized observational errors.

Supplementary Discussion

Supplementary Figure 10 shows zonal wind trends based on radiosondes and the ensemble mean of the six climate models for both time periods. Radiosondes and models show good agreement for both time periods (especially for 1970-2005), with a general increase in westerly wind, primarily above 300 hPa and poleward of ~30°N. Most of

these trends are significant at the 99% confidence level. These model results are similar to those based on CMIP2 experiments forced with CO_2 (1% $year^{-1}$ compounded)[6] and CMIP3 using SRES A2[7]. Differences exist near the equator, with radiosondes showing stronger negative trends than the model ensemble.

Supplementary Figure 11 shows the corresponding trends in observed and modeled westerly wind shear. Although the model ensemble shows more significant shear trends than the observations, there is generally good correspondence between models and observations, especially for 1970-2005. Most of the NH poleward of 30°N and above 500 hPa exhibits an increase in shear. Based on the thermal wind equation, this implies a corresponding increase in the meridional gradient of the mean temperature.

Supplementary Figure 12 shows NCEP/NCAR Reanalysis zonal wind and shear trends, which are quite different than those based on radiosondes and models (as apparent in Fig. 2). In the NH, except for two small regions near 40°N at 200-300 hPa and 70°N at 500 hPa, most wind and shear trends are negative. This may be due to the large volume of temperature data—which shows more tropospheric warming at mid-latitudes, relative to low latitudes—going into the reanalysis; for geostrophic balance to hold, wind shear must decrease.

Supplementary Figure 13 and 14 show zonal wind and shear seasonal trends for December-January-February (DJF) and June-July-August (JJA). For 1970-2005, the seasonal wind trends are generally similar to the annual trend (Supplementary Figure 10), with increasing zonal winds throughout most of the NH. DJF shows more significant increasing trends poleward of ~45°N in the troposphere; and an area of decreasing zonal wind trends between 25 to 45°N. This pattern is consistent with the positive phase of the

NAO/NAM[8]. In contrast, JJA shows a smaller area of increasing NH trends and larger increasing trends near 45°S. These results are consistent with increased tropospheric baroclinicity in the winter hemisphere.

For 1979-2005, the seasonal wind trends share fewer similarities with the annual trends. DJF shows a small region of increasing (decreasing) NH tropospheric trends centered at 60°N (45°N), again consistent with the positive phase of the NAO/NAM[8]. In the stratosphere, a large area of decreasing (increasing) trends exists between 40 and 70°N (10 and 40°N). In JJA, a decrease in stratospheric winds above 50 hPa throughout the NH exists and the region of increasing tropospheric annual westerlies in the NH has shifted poleward by ~15°. Similar to 1970-2005, SH JJA trends are larger than those in DJF.

Supplementary Figure 15 and 16 show seasonal wind-estimated temperature trends. Consistent with more increasing NH shear trends in DJF (Supplementary Figure 14), DJF exhibits more tropical upper tropospheric warming than JJA, for both time periods. The warming maximum is also stronger in SON, especially for 1979-2005. This suggests a role for atmospheric variability in altering the lapse rates on decadal time scales.

Supplementary Figure 17 compares 1979-2005 zonal temperature trends estimated from adjusted HadAT, RAOBCORE v1.4, and IUK temperature data ($\overline{T}_t$) derived from observed winds using the thermal wind equation ($\hat{\overline{T}}_t$), and estimated by models, for three layers of the atmosphere. Results are generally similar for the longer time period, 1970-2005, so only the satellite time period is discussed. In the troposphere (850-300 hPa), except for the large warming near 50°N, all models show warming that is essentially zonally-invariant, consistent with the $\overline{T}_t$ inferred from observed wind shear.

The mean model trend closely agrees with $\hat{\overline{T}}_t$. HadAT and IUK show substantially less warming in the tropics, consistent with previously published results[6]. RAOBCORE shows the most warming of the three homogenized data sets, but the tropical warming is still less than that based on the model ensemble and wind-estimated temperature.

For the 500-150 hPa layer, despite considerable $\overline{T}_t$ variability between models, all model results show a distinct pattern of $\overline{T}$ trend, with warming of the tropical upper troposphere/lower stratosphere relative to higher latitudes. The wind $\overline{T}$ trend also shows a similar profile, which falls within the spread of model predictions and closely resembles the ensemble mean. RAOBCORE also shows the warming of the tropical upper troposphere/lower stratosphere relative to higher latitudes. The $\overline{T}$ trend from IUK and HadAT once again shows negligible warming in the tropics, especially based on HadAT. This is inconsistent with all model results.

For the 150-100 hPa layer, models show warming throughout the tropics and subtropics, and cooling poleward of ~30-40°. This pattern of relative low latitude warming agrees with the wind-based $\overline{T}$ trends and RAOBCORE, which are particularly close to those predicted by the two GISS models. HadAT $\overline{T}$ trends show zonally-invariant cooling and bear little resemblance to the model ensembles or any individual model; these errors are somewhat improved in the IUK adjusted dataset.

Supplementary References

1 Thorne, P. W. et al. Revisiting radiosonde upper air temperatures from 1958 to 2002. *J. Geophys. Res.* **110**, doi:10.1029/2004JD005753 (2005).

2 Sherwood, S. C. Climate signals from station arrays with missing data, and an application to winds. *J. Geophys. Res.* **105**, 29489-29500 (2000).

3 Karl, T. R., Hassol, S. J., Miller, C. D. & Murray, W. L. (eds.). *Temperature Trends in the Lower Atmosphere: Steps for Understanding and Reconciling Differences* (A report by the Climate Change Science Program and the Subcommittee on Global Change Research, Washington, DC, 2006).

4 Santer, B. D. et al. Statistical significance of trends and trend differences in layer-average atmospheric temperature time series. *J. Geophys. Res*. **105**, 7337-7356 (2000).

5 Nakićenović, N. & Swart, R. (eds.). *Special Report on Emissions Scenarios. A Special Report of Working Group III of the Intergovernmental Panel on Climate Change* (Cambridge University Press, Cambridge, UK & New York, NY, 2000).

6 Raisanen, J. CO2-induced changes in the atmospheric angular momentum in CMIP2 experiments. *J. Clim*. **16**, 132-143 (2003).

7 Lorenz, D. J. & DeWeaver E. T. Tropopause height and zonal wind response to global warming in the IPCC scenario integrations. *J. Geophys. Res.* **112**, doi:10.1029/2006JD008087 (2007).

8 Thompson, D. W. J. & Wallace, J. M. Annular modes in the extratropical circulation. Part I: Month to month variability. *J. Clim.* **13**, 1000-1016 (2000).

Supplementary Figures

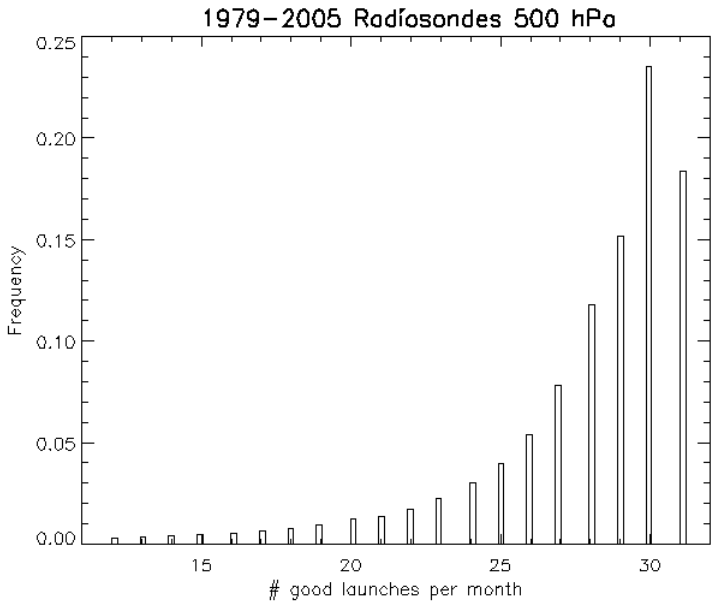

Supplementary Figure 1. The distribution of the number of valid radiosonde wind observations per month for 1979-2005 at 500 hPa.

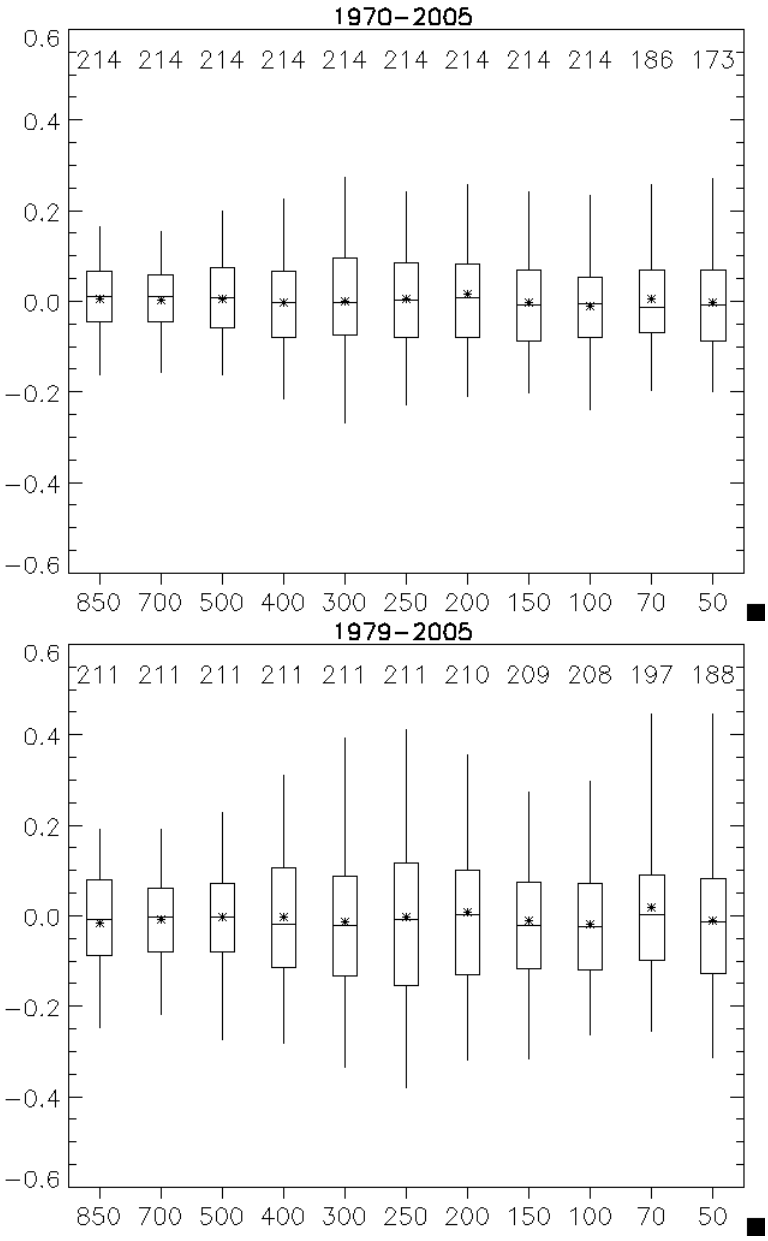

Supplementary Figure 2. Boxplots of 0000 UTC minus 1200 UTC radiosonde zonal wind trends for 1970-2005 (top panel) and 1979-2005 (bottom panel) for 11 pressure levels (bottom axis). The number at the top of each boxplot represents the number of stations used in the calculation. Each box plot shows the full range (whiskers); the inter-quartile range (top and bottom of each box); the median (horizontal line within each box); and the mean (asterisk).

12

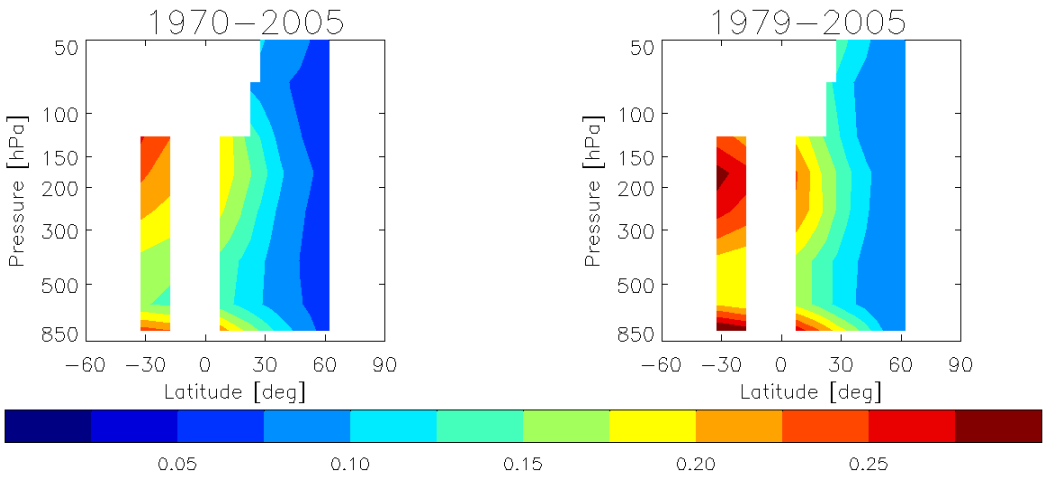

Supplementary Figure 3. The 2-σ sampling uncertainty in the wind-estimated $\overline{T}$ trend for the two time periods indicated. The integration constant at 62.5 °N is set to the 2-σ uncertainty of the trend of the zonal mean HadAT $\overline{T}$ based on 1000 realizations of the gridded zonally averaged time series. Units are K decade^{-1}.

13

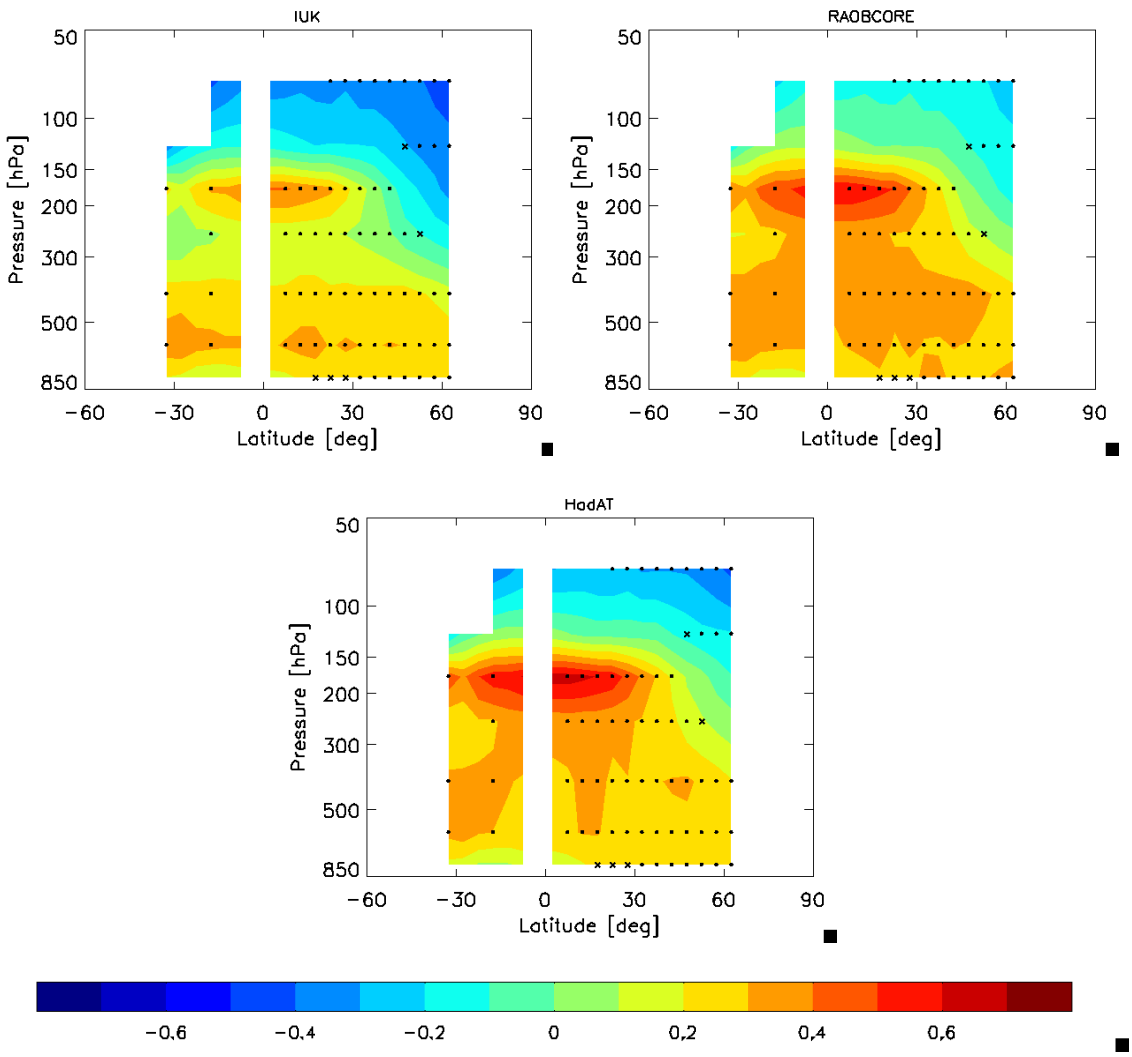

Supplementary Figure 4. Meridional sections of atmospheric warming trends estimated via (1) based on radiosonde winds for 1970-2005 using three different temperature data sets as the boundary condition at 62.5°N. The bottom panel is identical to Figure 3a. Symbols represent trend significance at the 95% (x) and 99% (dot) confidence level. Units are K decade^{-1}.

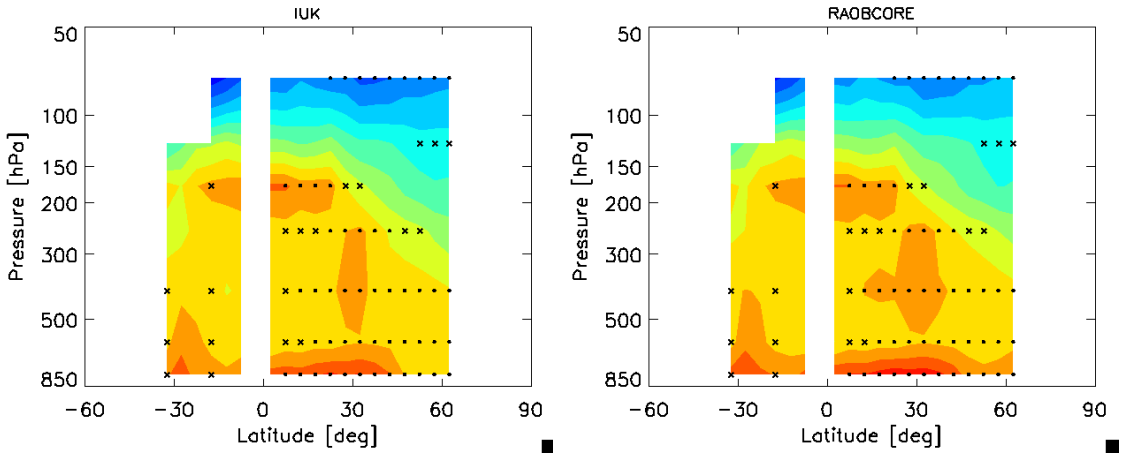

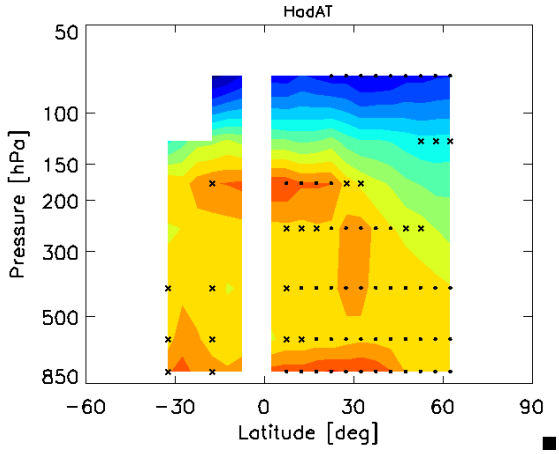

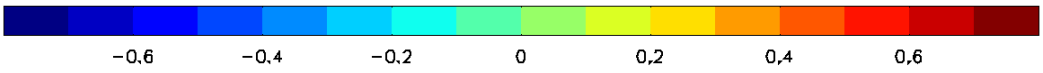

Supplementary Figure 5. As in Supplementary Figure 4, but for 1979-2005. The bottom panel is identical to Figure 3d.

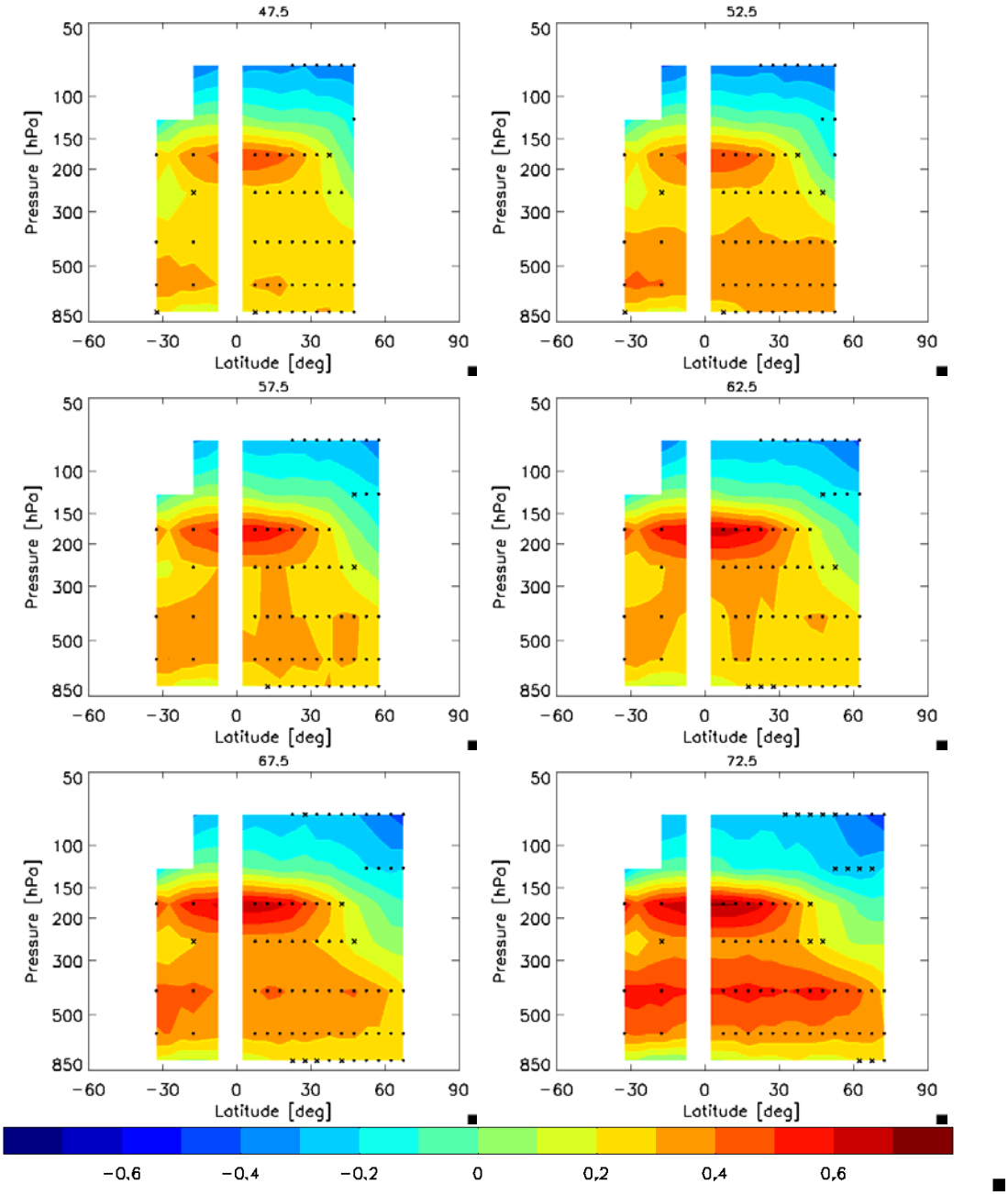

Supplementary Figure 6. Meridional sections of atmospheric warming trends estimated via (1) based on radiosonde winds for 1970-2005 using the adjusted HadAT zonal $\overline{T}$ trend at six different northern latitudes. The 62.5°N panel is identical to Figure 3a. Symbols represent trend significance at the 95% (x) and 99% (dot) confidence level. Units are K decade^{-1}.

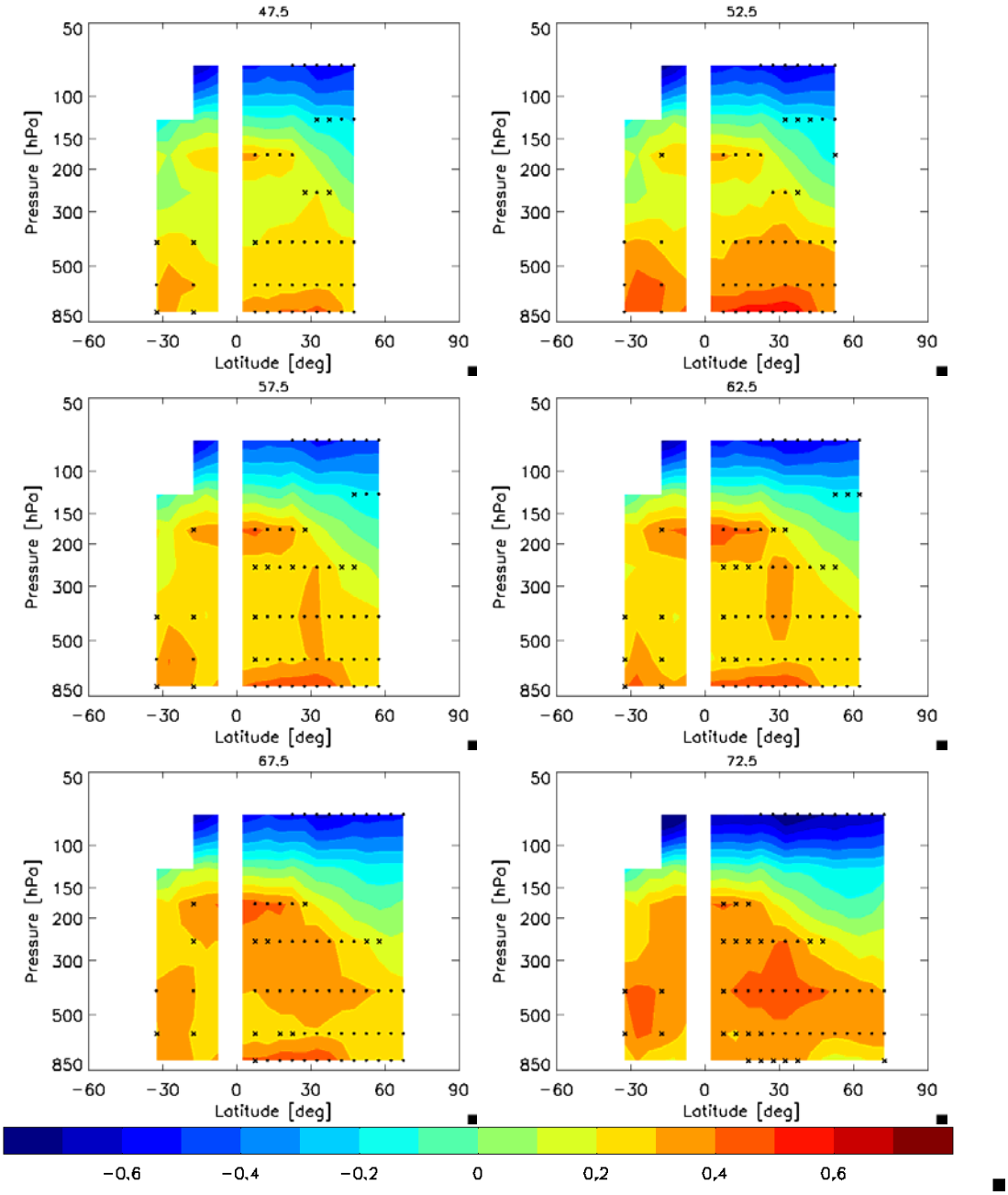

Supplementary Figure 7. As in Supplementary Figure 6, but for 1979-2005. The 62.5°N panel is identical to Figure 3d.

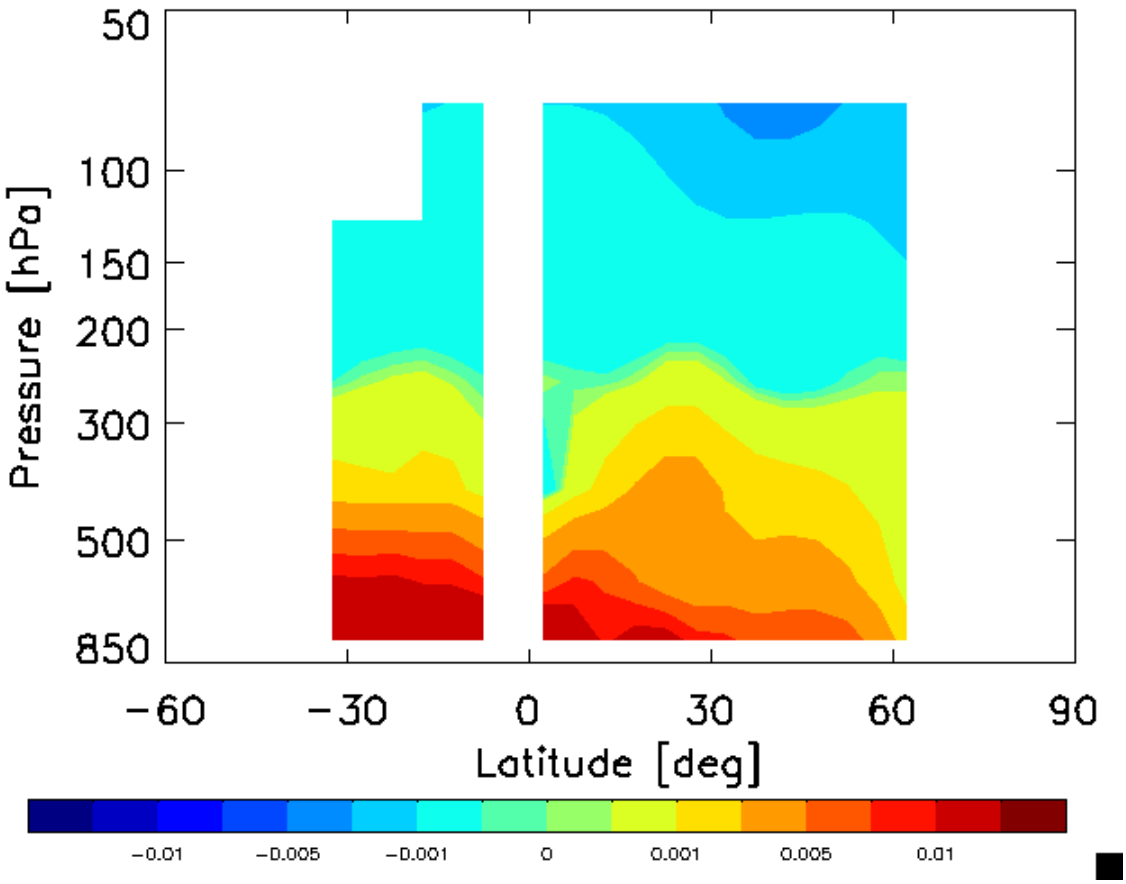

Supplementary Figure 8. Effect of moisture on the wind-estimated temperature trend for 1979-2005 (Fig. 3d). Units are K decade^{-1}.

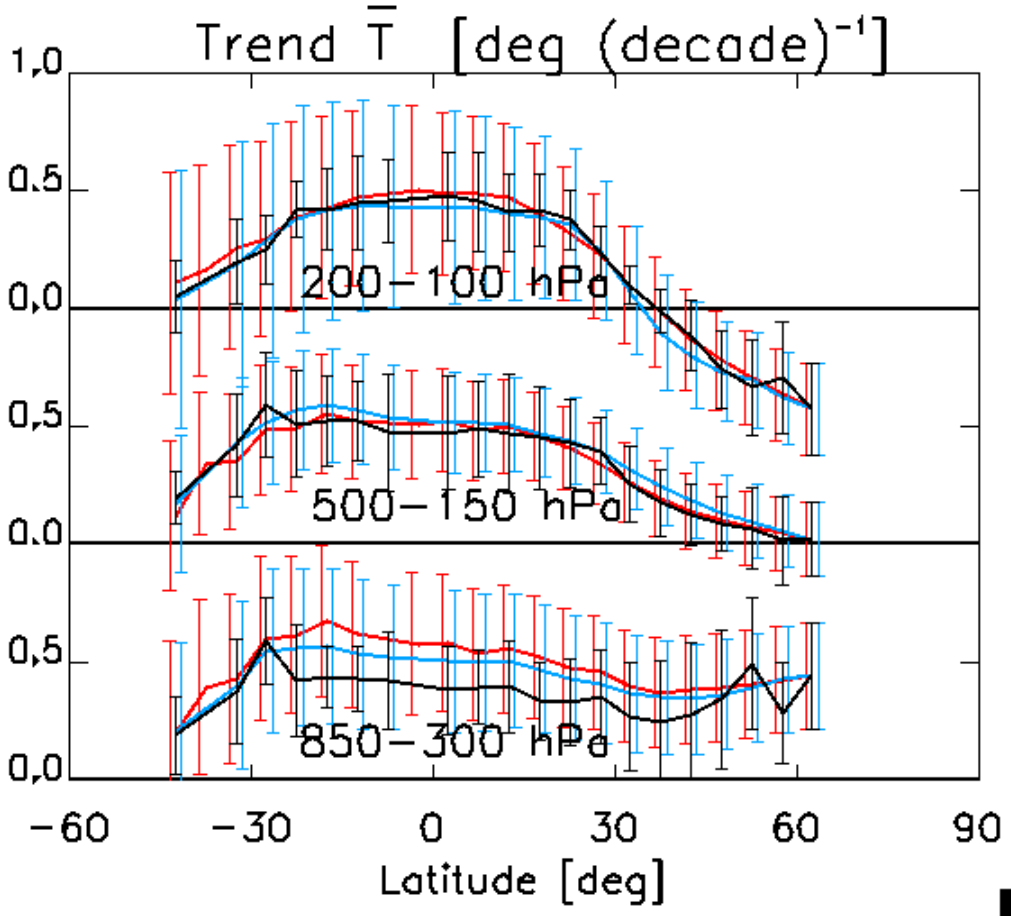

Supplementary Figure 9. Vertically averaged 1979-2005 zonal temperature trends for three layers (200-100 hPa; 500-150 hPa; 850-300 hPa) of the atmosphere based on MIROC3.2 (hires). Trends are based on the model's actual temperatures (black); integration of the meridional temperature gradient (red) and the vertical wind shear (navy) using the thermal wind equation. Trends for 200-100 hPa (850-300 hPa) are offset vertically by 1° decade^{-1} (-1° decade^{-1}) as indicated by the horizontal lines. The model has been masked with the same missing monthly data as the gridded radiosonde winds. Trends based on the meridional temperature gradient and vertical wind shear are set to the model's actual temperature trend at the northernmost grid point (62.5°N). Error bars indicate the 2-σ uncertainty in the estimated linear trend.

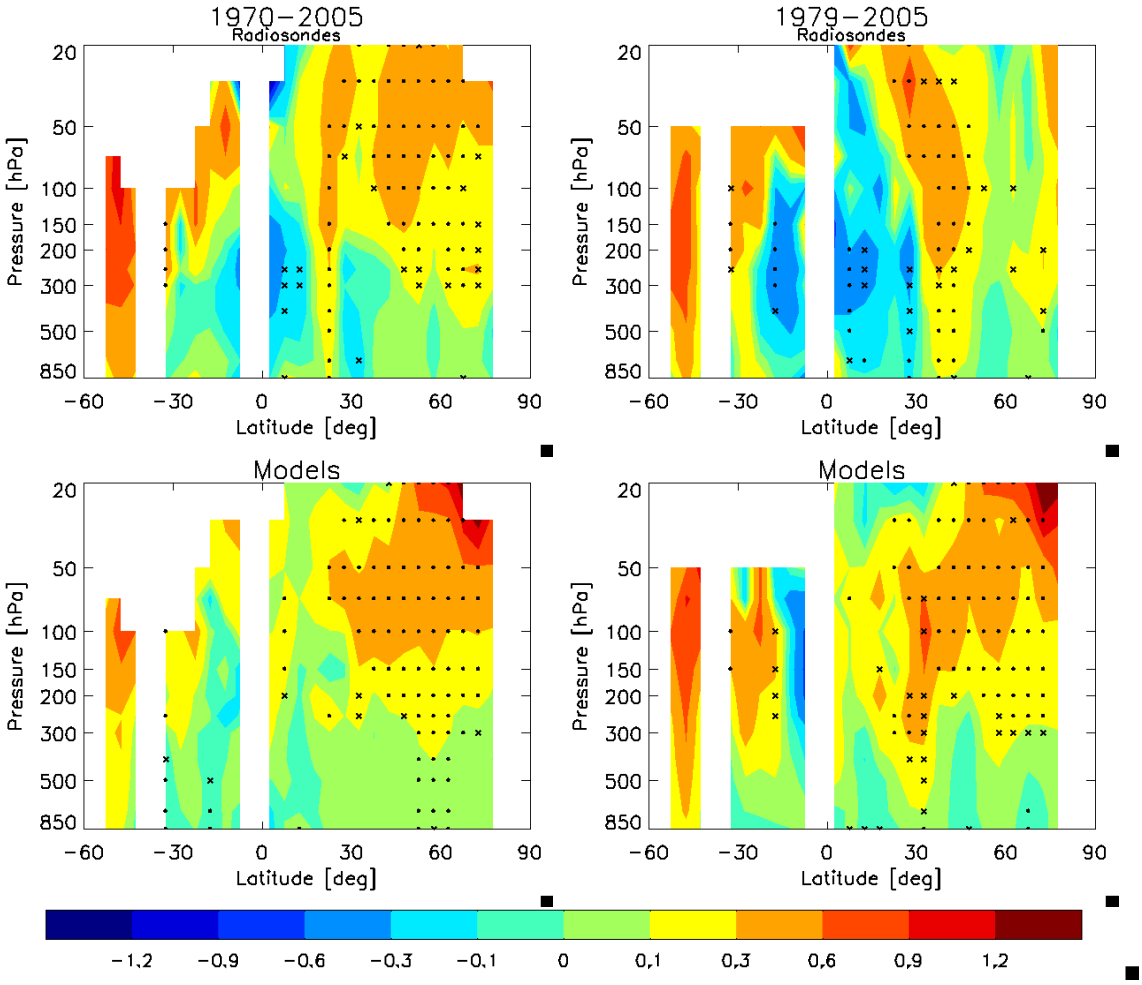

Supplementary Figure 10. Trends in observed (top panel) zonal mean westerly wind for 1970-2005 (left panel) and 1979-2005 (right panel). Also included is the mean from the six climate models (bottom panel) discussed in the main text. Symbols represent trend significance at the 95% (x) and 99% (dot) confidence level based on a two-tailed Student's t-distribution test. Units are m [s-decade]$^{-1}$. The 1979-2005 radiosonde wind trend plot (top right panel) is identical to Fig. 1a.

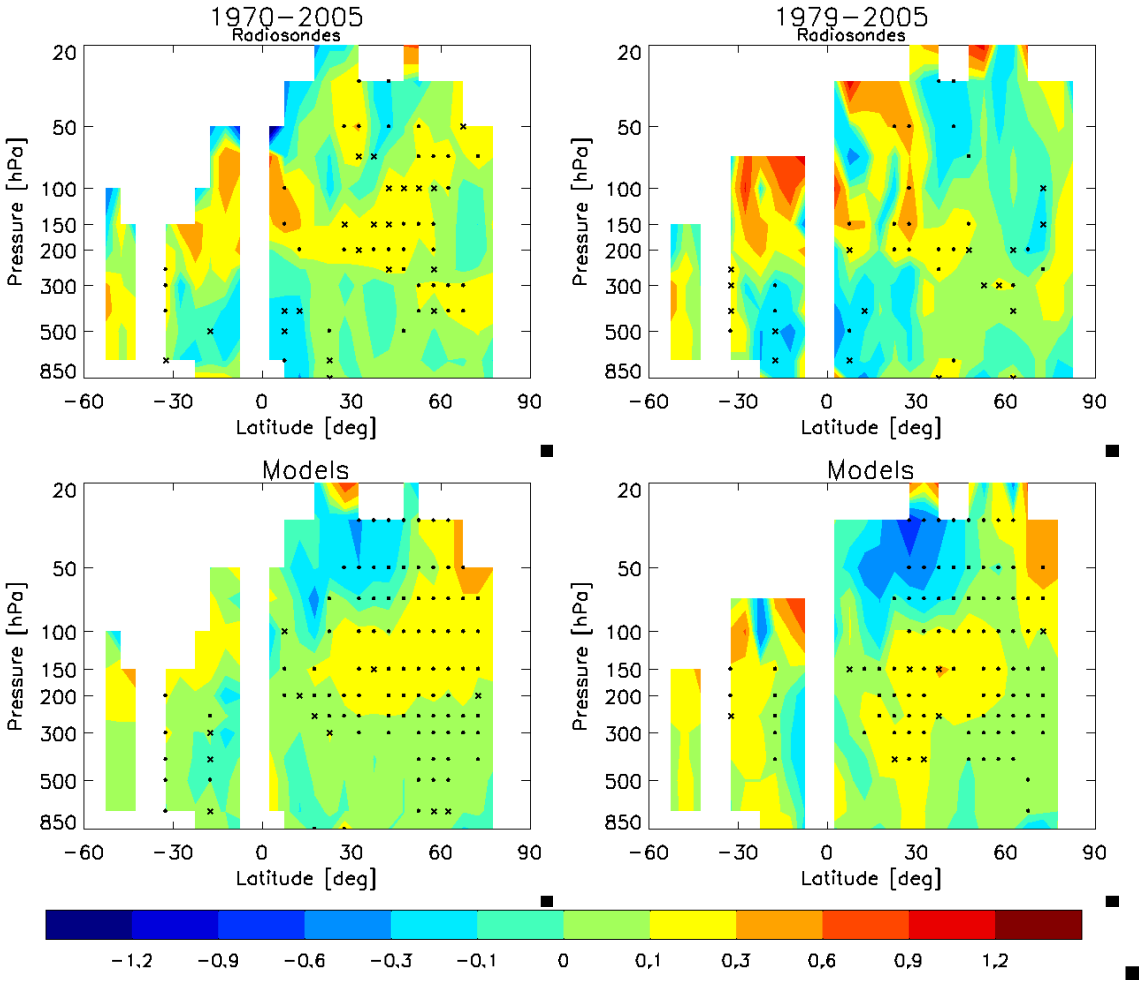

Supplementary Figure 11. As in Supplementary Figure 10, but based on trends in zonal mean westerly wind shear. The 1979-2005 radiosonde shear trend plot (top right panel) is identical to Fig. 1b.

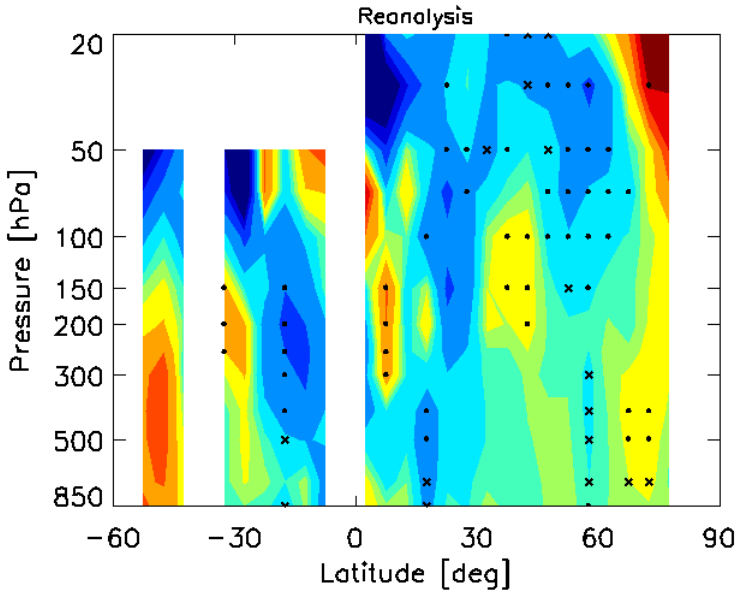

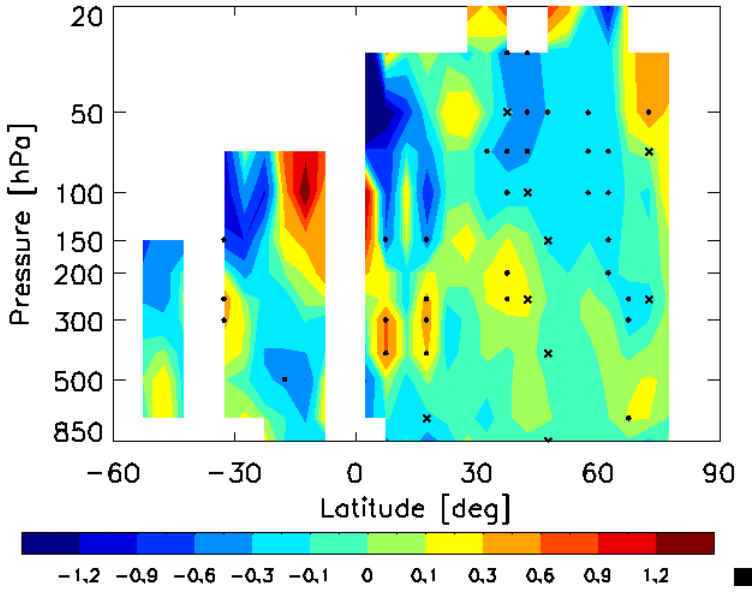

Supplementary Figure 12. Zonal trends in zonal wind (top panel) and shear (bottom panel) for 1979-2005 based on NCEP/NCAR Reanalysis, masked with the same missing monthly data as the gridded radiosonde wind. Symbols represent trend significance at the 95% (x) and 99% (dot) confidence level based on a two-tailed Student's t-distribution test with 26 degrees of freedom. Units are m [s-decade]$^{-1}$.

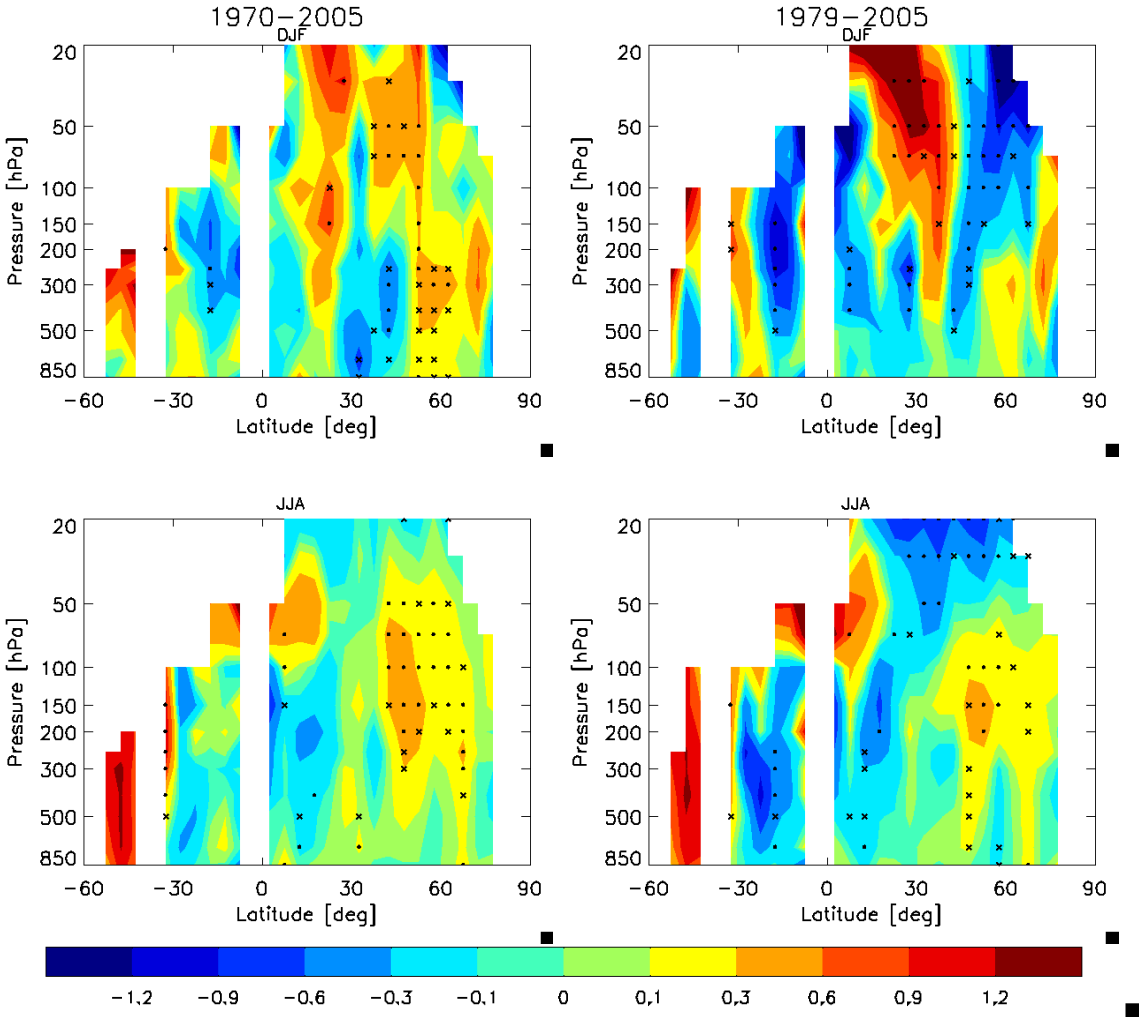

Supplementary Figure 13. Seasonal trends in observed zonal mean westerly wind for DJF (top panel) and JJA (bottom panel) for the two time periods indicated. Symbols represent trend significance at the 95% (x) and 99% (dot) confidence level based on a two-tailed Student's t-distribution. Units are m [s-decade]$^{-1}$.

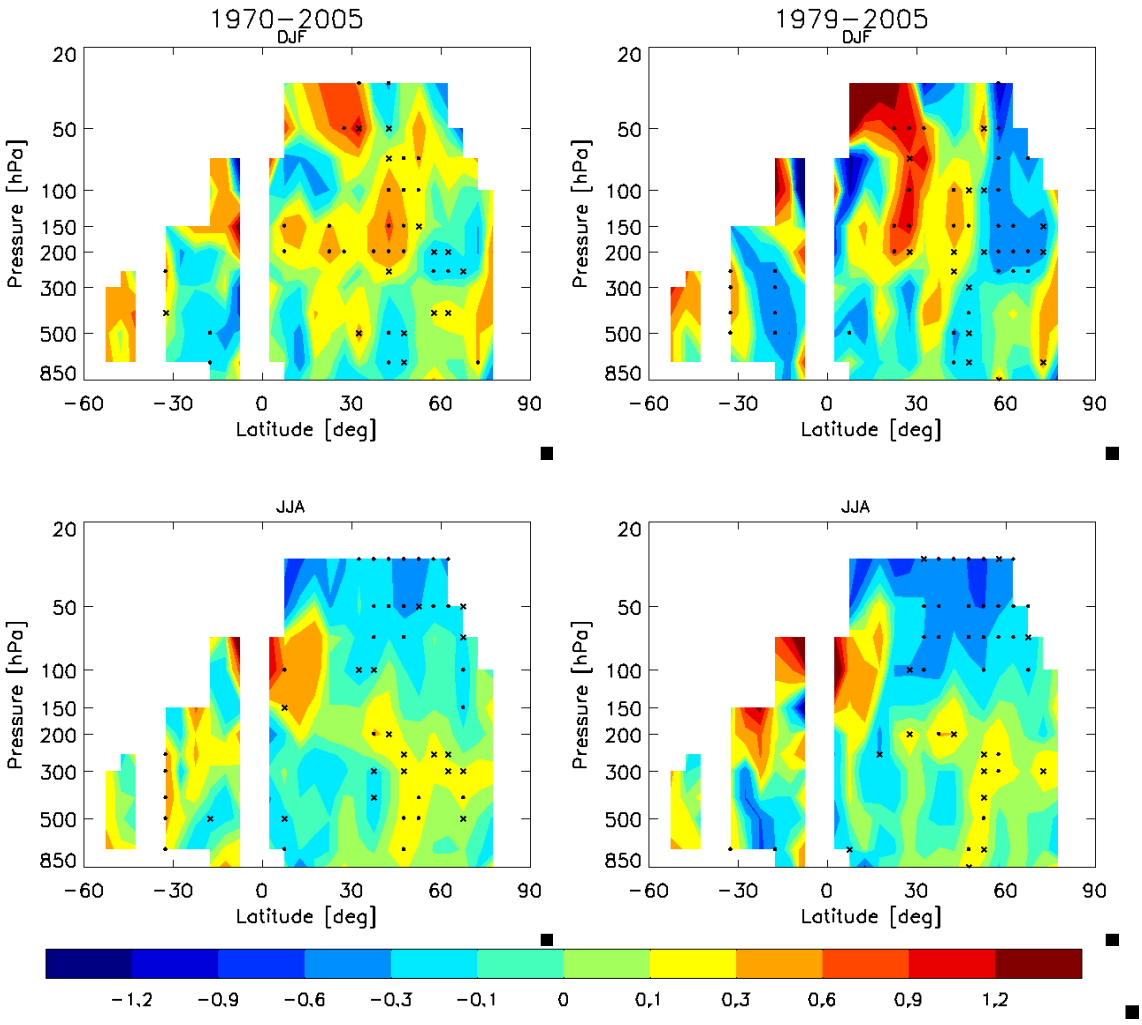

Supplementary Figure 14. As in Supplementary Figure 13, but based on trends in zonal mean westerly wind shear.

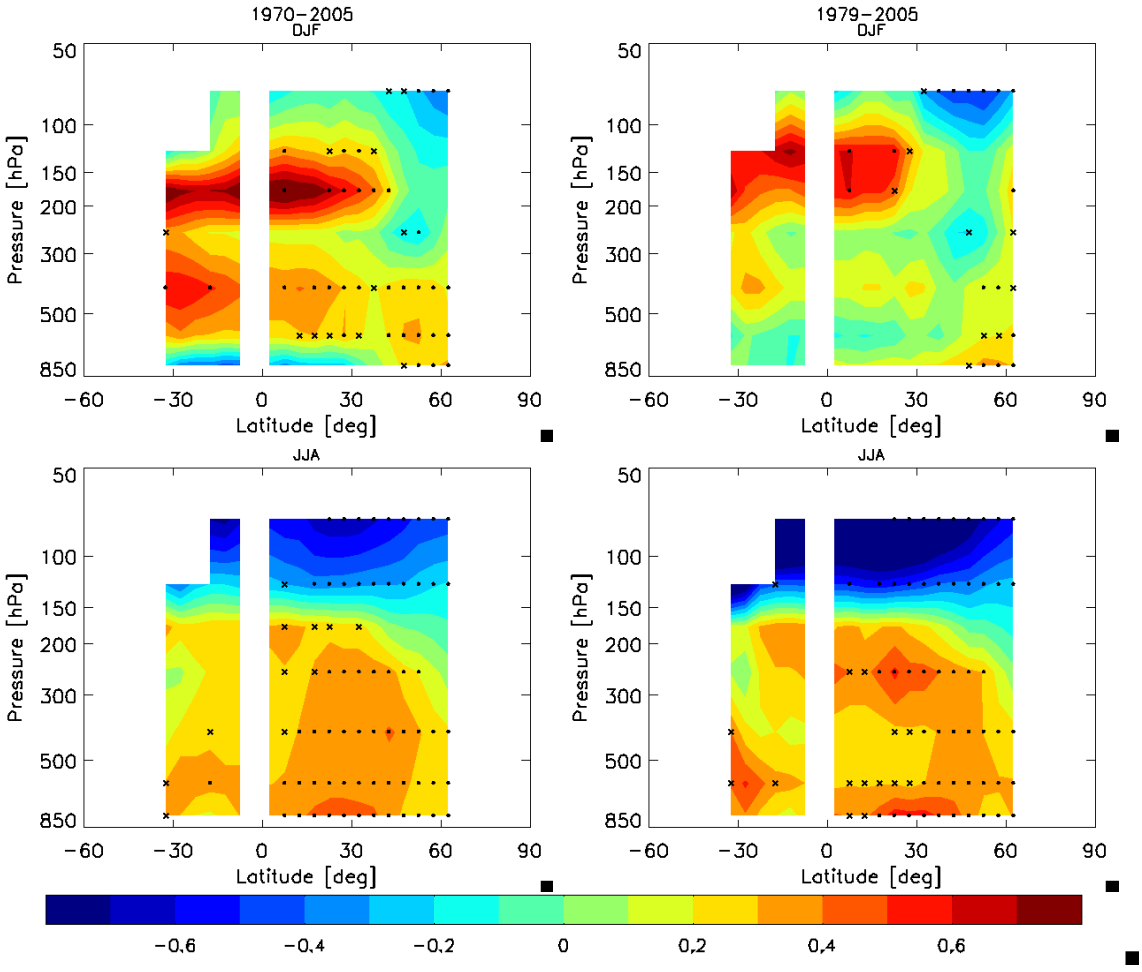

Supplementary Figure 15. Seasonal trends in wind-estimated temperature for DJF (top panel) and JJA (bottom panel) for the two time periods indicated. Symbols represent trend significance at the 95% (x) and 99% (dot) confidence level based on a two-tailed Student's t-distribution. Units are K decade^{-1}.

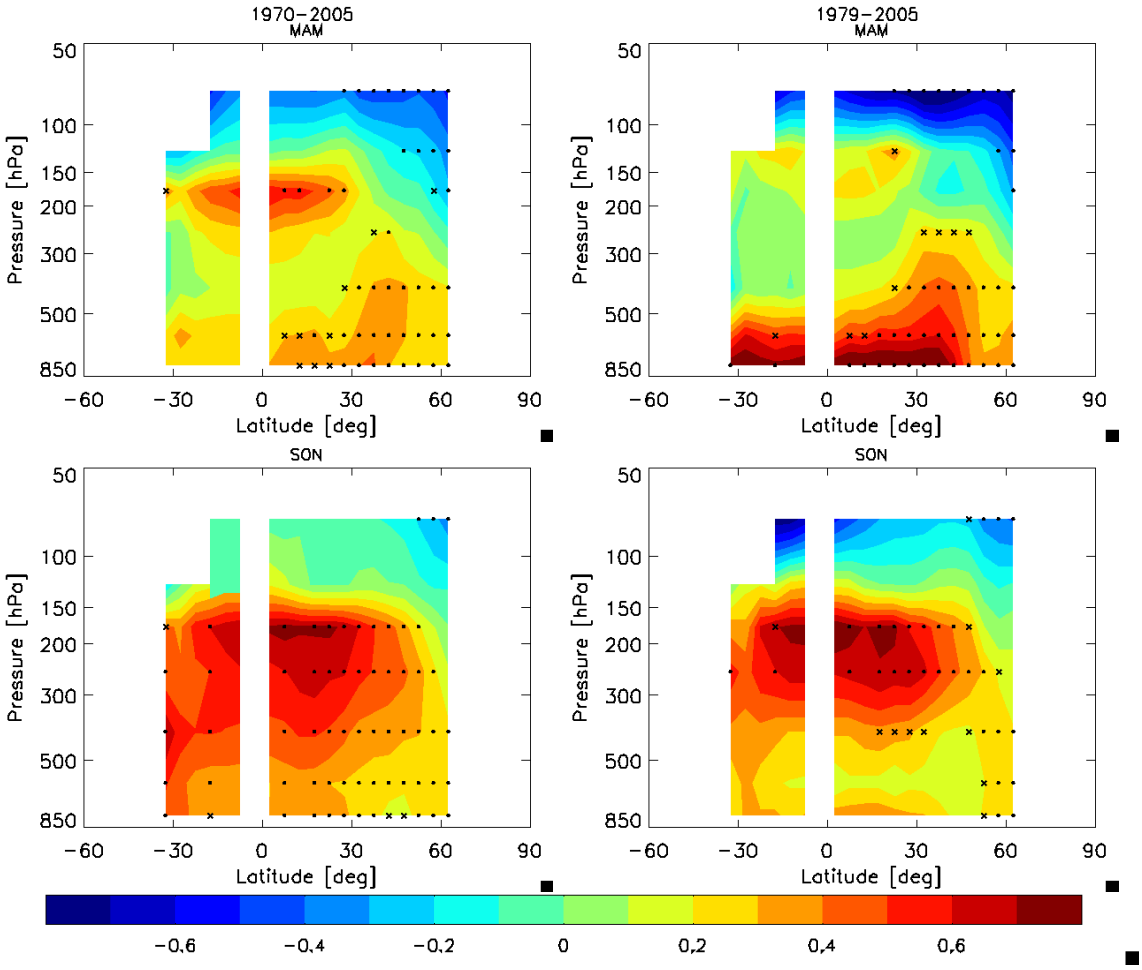

Supplementary Figure 16. As in Supplementary Figure 15, but for MAM (top panel) and SON (bottom panel).

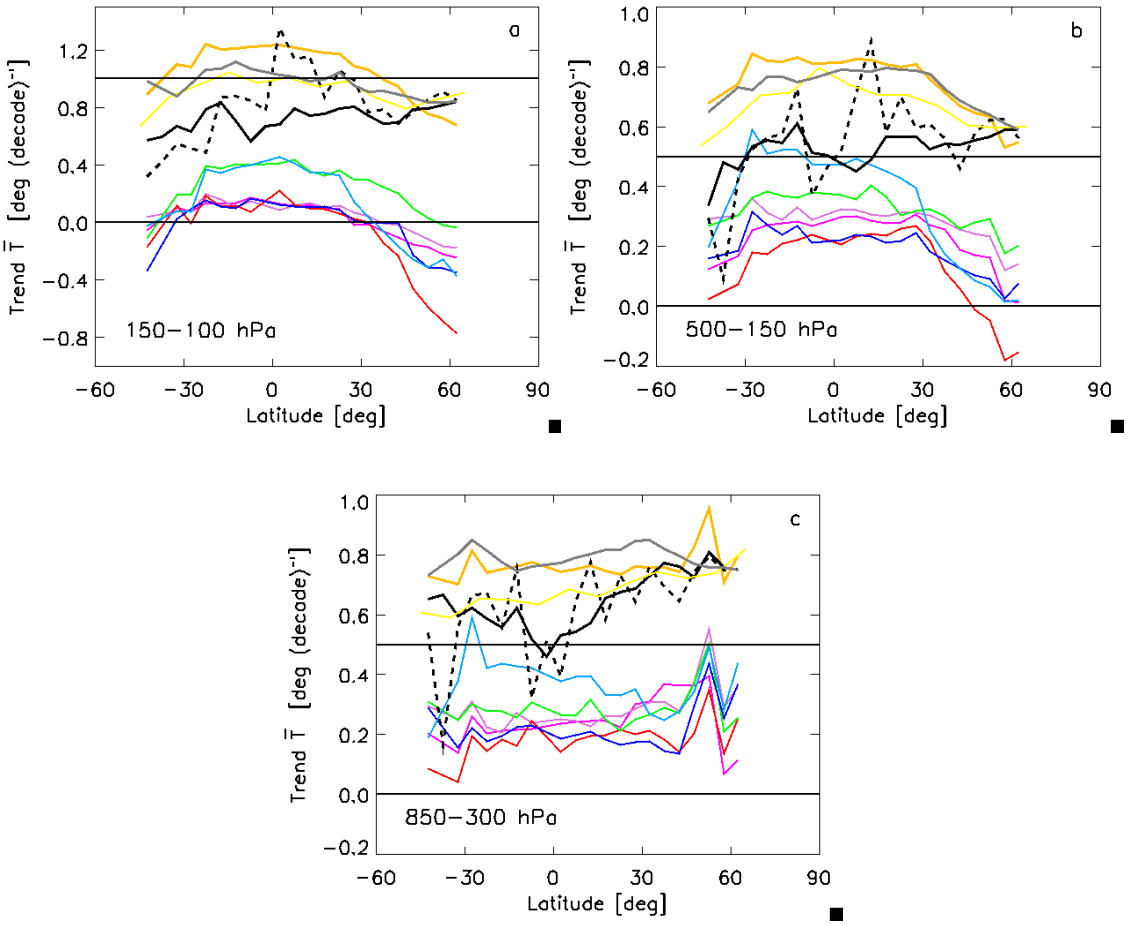

Supplementary Figure 17. Zonal $\overline{T}$ trends for 1979-2005 of model temperature, HadAT (solid black), IUK (dashed black) and RAOBCORE v1.4 (yellow) adjusted temperature, and wind-estimated temperature (gray) for three layers. Individual realizations are shown for UKMO-HadCM3 (red), GISS-EH (light purple), GISS-ER (dark purple), CNRM-CM3 (green), MIROC3.2 (medres) (blue), and MIROC3.2 (hires) (navy). The average of these six models (orange) is also shown. Model ensembles and observations are offset +1.0° decade^{-1} in panel a and +0.5° decade^{-1} in panels b and c, for clarity. Wind estimated $\overline{T}_t$ are set to the adjusted HadAT $\overline{T}_t$ at 62.5°N.

Supplementary Table 1. Definition of coupled climate model acronyms from the IPCC Fourth Assessment Report used in this study. The first six models comprise the ensemble means shown in this analysis and constitute those models that predict surface warming in the tropics similar in magnitude to that observed. The remaining three models are used in the supplement to show the range of model simulated warming.

Model Acronym	Country	Institution
CNRM-CM3	France	Meteo-France/Centre National de Recherches Meteorologiques
GISS-EH	United States	Goddard Institute for Space Studies
GISS-ER	United States	Goddard Institute for Space Studies
MIROC3.2 medres	Japan	Center for Climate System Research/NIES[a]/JAMSTEC[b]
MIROC3.2 hires	Japan	Center for Climate System Research/NIES[a]/JAMSTEC[b]
UKMO-HadCM3	United Kingdom	Hadley Center for Climate Prediction and Research
CCCma-CGCM3.1(T63)	Canada	Canadian Center for Climate Modeling and Analysis
GFDL-CM2.1	United States	Geophysical Fluid Dynamics Laboratory
UKMO-HadGEM1	United Kingdom	Hadley Center for Climate Prediction and Research

a. NIES is the National Institute for Environmental Studies
b. JAMSTEC is the Frontier Research Center for Global Change in Japan